JACS
JOURNAL OF THE AMERICAN CHEMICAL SOCIETY
Article
pubs.acs.org/JACS

Fluorinated Benzothiadiazole-Based Conjugated Polymers for High-Performance Polymer Solar Cells without Any Processing Additives or Post-treatments

Ning Wang,[‡] Zheng Chen,*[,†] Wei Wei,[†] and Zhenhua Jiang[†]

[†]Alan G. MacDiarmid Lab, College of Chemistry, Jilin University, Xiuzheng Road 1788, Changchun 130012, People's Republic of China

[‡]Changchun Institute of Applied Chemistry, Chinese Academy of Sciences, Renmin Str. 5625, Changchun 130022, People's Republic of China

Supporting Information

ABSTRACT: Thanks to their many favorable advantages, polymer solar cells exhibit great potential for next-generation clean energy sources. Herein, we have successfully designed and synthesized a series of new fluorinated benzothiadiazole-based conjugated copolymers $PBDT_{TEH}$-$DT_{H}BTff$ (**P1**), $PBDT_{TEH}$-$DT_{EH}BTff$ (**P2**), and $PBDT_{HDO}$-$DT_{H}BTff$ (**P3**). The power conversion efficiencies of 4.46, 6.20, and 8.30% were achieved for **P1**-, **P2**-, and **P3**-based devices within ~100 nm thickness active layers under AM 1.5G illumination without any processing additives or post-treatments, respectively. The PCE of 8.30% for **P3** is the highest value for the reported traditional single-junction polymer solar cells via a simple fabrication architecture without any additives or post-treatments. In addition, it is noteworthy that **P3** also allows making high efficient polymer solar cells with high PCEs of 7.27 and 6.56% under the same condition for ~200 and ~300 nm thickness active layers, respectively. Excellent photoelectric properties and good solubility make polymer **P3** become an alternative material for high-performance polymer solar cells.

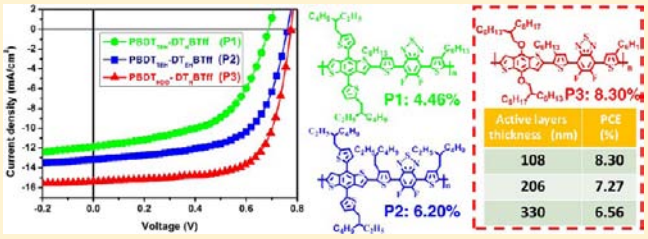

1. INTRODUCTION

On account of their distinctive potential for fabricating flexible, lightweight, large-area, and low-cost devices through roll-to-roll coating processes,[1−3] polymer solar cells (PSCs) based on bulk heterojunction (BHJ) architecture have attracted much attention. In this field, rapid and significant progress has been realized in the past decade; the power conversion efficiencies (PCEs) of traditional single-junction PSCs have reached 8% by optimizing material band gaps, carrier mobilities and energy levels, and regulating nanoscale morphologies of active networks.[4−13] Up to date, the PCEs of tandem BHJ PSCs have broken 10% milestone.[14] Meanwhile, important progress is achieved in roll-to-roll processes for large-scale fabrication of PSCs.[15] The desired ideal materials combining high PCE with convenient processability become urgent for PSCs to meet the commercial requirements.[3,16] Therefore, a promising candidate polymer possessing high efficiency with simple fabrication process is very much in demand for developing high-performance large-scale industry printing applications of PSCs.[17,18]

In order to achieve high-performance PSCs, a successful and universal strategy is to design donor−acceptor (D−A) alternating copolymers combined electron-rich (donor) and electron-deficient (acceptor) moieties, which can tune the energy levels and absorption properties by controlling the intermolecular charge transferring from the donor to the acceptor. Recently, many kinds of D−A copolymers have been developed and showed good photovoltaic properties with PCEs as high as 8% in single-junction PSCs.[4,8,11−13] However, to obtain high PCEs in above-mentioned materials, processing additives or post-treatments were usually employed to optimize the device performance.[4−11]

Recently, fluorine atoms substituted directly to the backbone of conjugated polymers have showed great promise in enhancing efficiency of BHJ PSCs.[19−28] Inserting fluorine atoms on acceptor units can improve the key factors of PCE including open-circuit voltage (V_{oc}), short-circuit current density (J_{sc}), and fill factor (FF).[20] As a result, as an electron-withdrawing unit, 4,7-di(thien-2-yl)-5,6-difluoro-2,1,3-benzothiadiazole (DTBTff)-based copolymers have attracted much attention.[24,28] Among these works, Wei You et al. achieved a high efficiency device based on benzothiadiazole copolymer with a PCE up to 7.2% without using additives.[24] Although this polymer was disturbed with limited solubility in common organic solvent at room temperature, the great potential of BDT-DTBTff (D−A) structure polymer was shown. It is well-known that side chains play a crucial role in certain key properties of conjugated polymers, such as molecular weight, inter- and intramolecular interactions, charge transport, and

Received: August 1, 2013
Published: October 22, 2013

   dx.doi.org/10.1021/ja409881g | J. Am. Chem. Soc. 2013, 135, 17060−17068

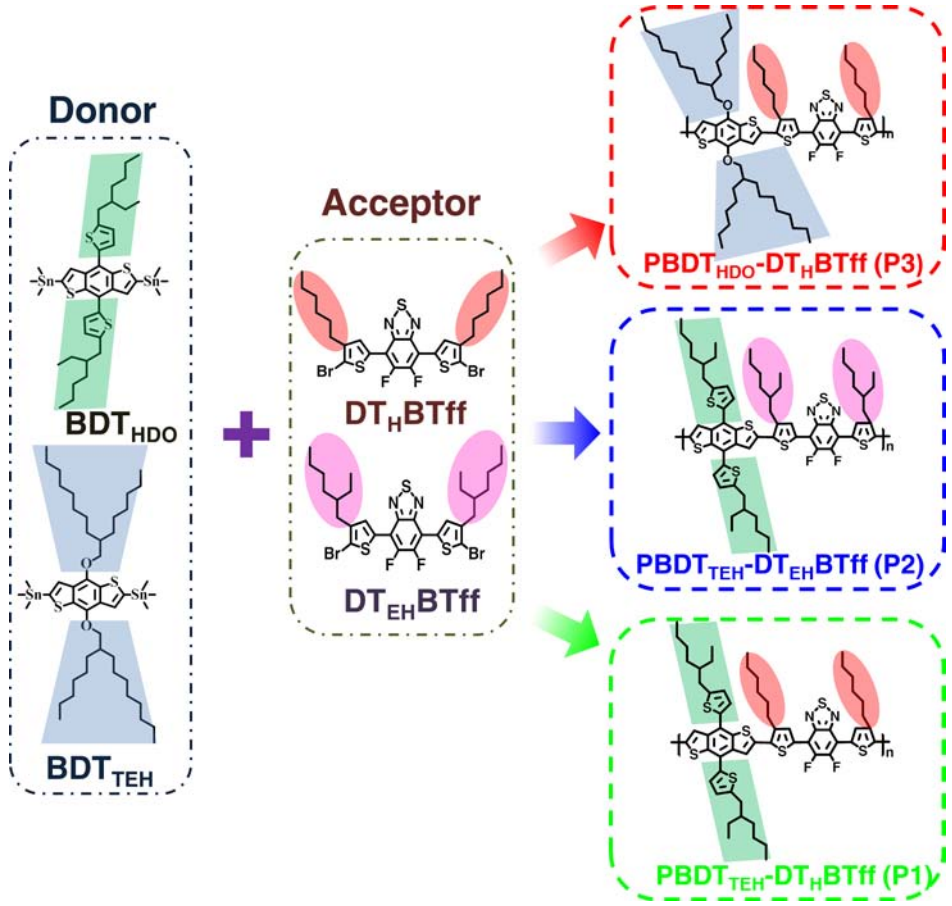

Figure 1. Design and synthesis of a series of new fluorinated benzothiadiazole-based copolymers **P1**, **P2**, and **P3**.

active layer morphology.[16,29] Selecting proper side chains can adjust intermolecular interactions and allow proper blending with [6,6]phenyl-C_{61}-butyric acid methyl ester ($PC_{61}BM$)/[6,6] phenyl-C_{71}-butyric acid methyl ester ($PC_{71}BM$) to form desired morphology,[13] and the excellent solubility is benefiting to obtain good film quality and desired phase morphologies of active layers. Consequently, the key factors of PCE including V_{oc}, J_{sc}, and FF also can be tuned by selecting proper side chains on benzo[1,2-b:4,5-b′]dithiophene (BDT) units.[11,16,19,30−32]

In our group, we primarily focus on developing high-performance polymers for PSCs combining with high efficiency and simple processability. For this reason, we have explored and developed a series of new polymers based on BDT-DTBTff (D−A) main chain structure. In order to improve PCE of PSC, we tried to introduce two kinds of side chains into copolymers main chains (Figure 1). First, we introduced alkylthienyl into BDT units to form two-dimensional conjugated (2D-conjugated) (Scheme 1). As well-known, the two-dimensional conjugated (2D-conjugated) polymers possess higher hole mobility due to the 2D-conjugated structure and broader absorption deriving from both main chains and conjugated side chains.[30] Second, we introduced bulk branched alkoxyl side chains into the BDT units to try to realize the improvement both of solubility and J_{sc}.[11,19] Actually, most of synthetic chemists enjoy employing bulk branched alkyl groups as solubilizing side chains to replace alkoxy groups on BDT units for lowering HOMO levels of low band gap polymers.[20,24,26,28] It is noteworthy that inserting the electron-donating oxygen atoms to the donor units also can enhance J_{sc} and FF of devices, although moderate decrease in V_{oc} in some degree.[11,19,24,33]

In this paper, we have successfully designed and synthesized a series of new fluorinated benzothiadiazole conjugated copolymers (Scheme 1) with two distinctive side chains on BDT units. By contrast research, we have investigated the effects of the two side chains on device performance in detail. It should be pointed out that **P3** showed good solubility in common organic solvent at room temperature in our experiments. PCEs of 4.46, 6.20, and 8.30% were achieved for PBDT$_{TEH}$-DT$_H$BTff (**P1**), PBDT$_{TEH}$-DT$_{EH}$BTff (**P2**) and PBDT$_{HDO}$-DT$_H$BTff (**P3**) based devices within ∼100 nm thickness active layers under AM 1.5G illumination without any processing additives or post-treatments, respectively. To the best of our knowledge, the PCE of 8.3% is the highest value for traditional single-junction PSCs without any additives or post-treatments. Furthermore, the devices based on **P3** also showed favorable performance with thick photoactive layers above 200 nm.

2. RESULTS AND DISCUSSION

Synthesis of Monomers and Polymers. While monomers 2,6-bis(trimethyltin)-4,8-bis(5-(2-ethylhexyl)thiophen-2-yl)benzo-[1, 2-b:4,5-b′]dithiophene (BDT$_{TEH}$) and 5,6-difluoro-4,7-bis-(5-bromo-4-(2-ethylhexyl)-2-thienyl)-2,1,3-benzothiadiazole (DT$_{EH}$BTff) were synthesized according to literature reports,[24,28,30] the synthesis of the 2,6-bis-(trimethylstannyl)-4,8-bis(hexyldecyloxy)-benzo[1,2-b:4,5-b′]-dithiophene (BD-T$_{HDO}$) and 4,7-bis(5-bromo-4-hexylthienyl)-

dx.doi.org/10.1021/ja409881g | J. Am. Chem. Soc. 2013, 135, 17060−17068

Scheme 1. Synthesis of Monomers (BDT_{HDO}, BDT_{TEH}, DT_HBTff, and $DT_{HB}Tff$) and Conjugated Copolymers ($PBDT_{TEH}$-DT_HBTff (P1), $PBDT_{TEH}$-$DT_{EH}BTff$ (P2), and $PBDT_{HDO}$-DT_HBTff (P3))

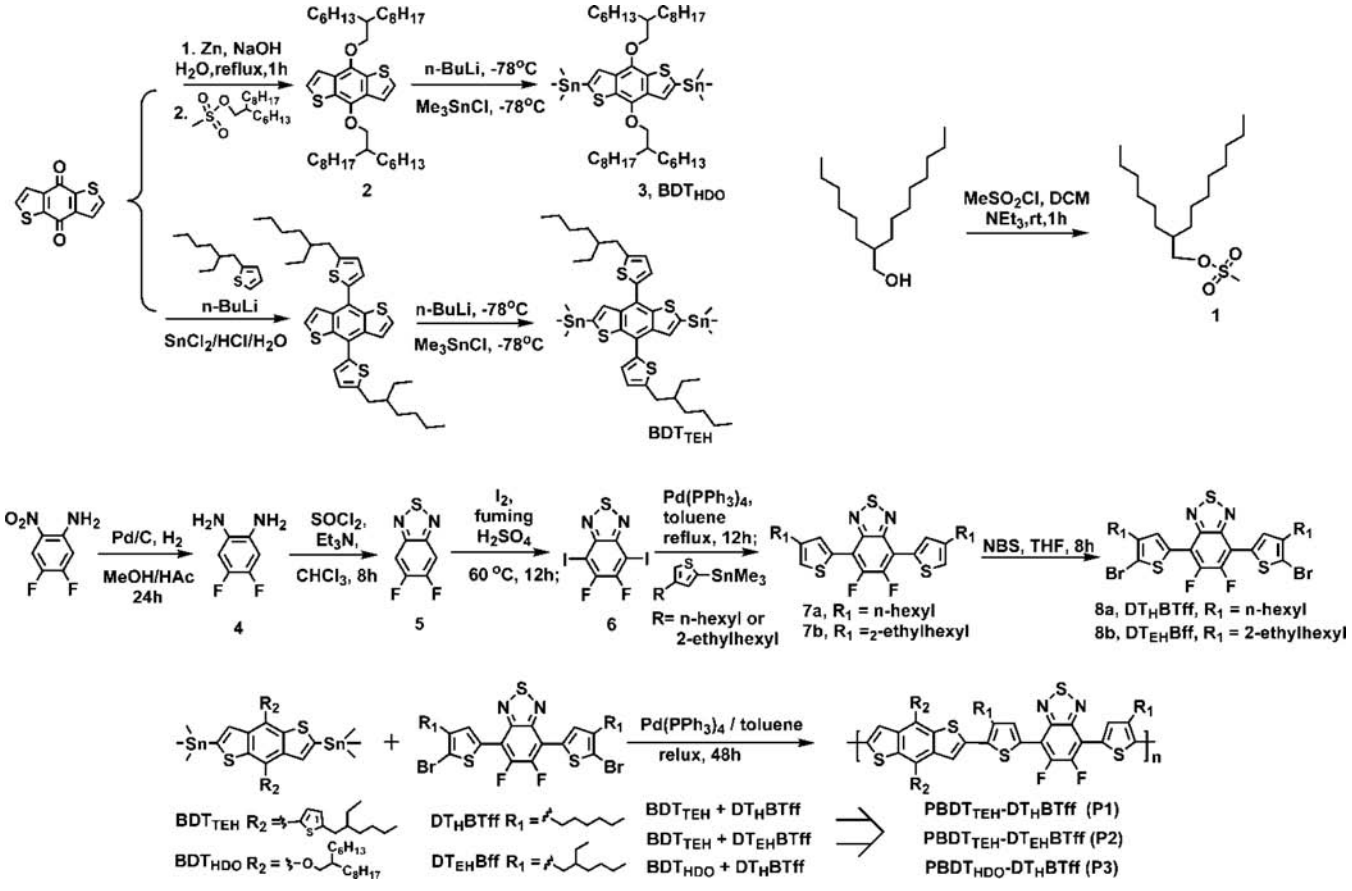

Table 1. Basic Properties of Polymer (Molecular Weight, Thermostability, Optical and Electrochemical Properties)

					λ_{max} [nm]		λ_{edge} [nm]					
polymer	M_n (kDa)[a]	PDI	T_g (°C)	$T_{d\,5\%}$ (°C)	solution	film	solution	film	HOMO (eV)	LUMO (eV)	E_g^{opt} (eV)[b]	E_g^{cv} (eV)[c]
P1	14.5	2.0	–	442	449, 586	450, 595	715	720	−5.33	−3.12	1.72	2.21
P2	22.2	1.5	–	434	442, 580	441, 590	700	707	−5.34	−3.08	1.76	2.26
P3	27.5	1.8	138	321	413, 550	427, 626	673	730	−5.31	−3.20	1.70	2.11

[a]Determined by GPC in 1,2,4-trichlorobenzene at 120 °C. [b]Measured by cyclic voltammetry. [c]Band gaps were calculated from the onset of the film absorption.

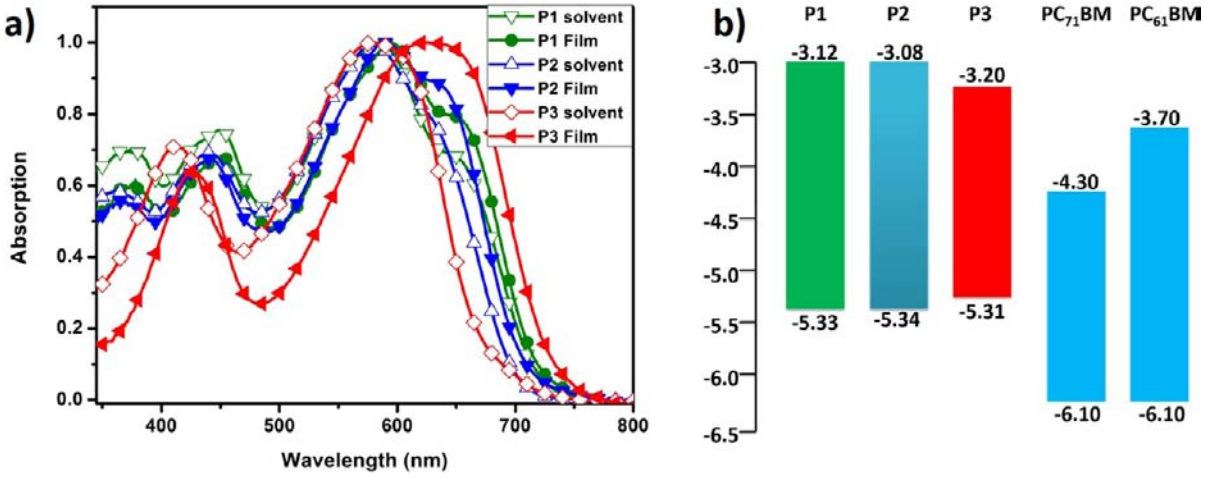

Figure 2. (a) UV−vis absorption spectra of the polymers in solution and thin films. (b) HOMO and LUMO energy levels of the polymers.

dx.doi.org/10.1021/ja409881g | J. Am. Chem. Soc. 2013, 135, 17060−17068

5,6-difluoro-2,1,3-benzothiadiazole (DT_HBTff) were depicted in Supporting Information. As described in Scheme 1, **P1**, **P2**, and **P3** were synthesized by Stille coupling in high yields; palladium tetrakis(triphenylphosphine) ($Pd(PPh_3)_4$) was used as catalyst (Scheme 1). All polymers were carefully purified by extracting with methanol, hexanes, tetrahydrofuran, and chloroform to remove oligmers and other small molecular parts. The solubility is different among these polymers. **P3** can dissolve in chloroform, toluene and 1,2,4-trichlorobenzene (TCB) at room temperature, **P2** also can dissolve completely in these solvent at elevated temperature, and **P1** only can dissolve partly in toluene and 1,2,4-trichlorobenzene (TCB) at elevated temperature. Number-average molecular weights (M_n) and polydispersity index (PDI, M_n/M_w) were obtained from high-temperature size-exclusion chromatography (SEC) using TCB at 120 °C as the eluent (Table 1).

Optical and Electrochemical Properties. The normalized UV−visible absorption spectra of three polymers **P1**, **P2**, and **P3** in chlorobenzene solution and thin films are shown in Figure 2a. And the absorption data were collected and listed in Table 1. These polymers show very similar absorption bands in chlorobenzene solution with major absorption peaks at 586 nm for **P1**, 580 nm for **P2**, and 579 nm for **P3**. This typical band can be assigned to the intramolecular charge transfer interaction between electron-rich and -deficient units. The other band in short-wavelength near 400 nm can be assigned to 4,7-dithien-2-yl-2,1,3-benzothiadiazole (DTBT) units, which were often observed in DTBT containing conjugated polymers.[28,34,35] In the solid state, the main absorption peaks become broader, and the red shifts occur toward longer wavelength with maximum absorption peaks at 595 nm for **P1**, 590 nm for **P2**, and 626 nm for **P3**. These large red shifts from solution to solid state means more coplanar structure and stronger interchain $\pi-\pi$ stacking in the solid state. It is interesting that the red shifts of **P1** and **P2** were only ∼10 nm from solution to films. On the contrary, **P3** showed bigger red shift with 47 nm than **P1** and **P2** in solid state, thus leading to a broader absorption. These results may originate from larger steric hindrance structures in **P1** and **P2**. In addition, two shoulder peaks appeared near 630 nm both in solution and solid states for **P1** and **P2**. The optical band gaps were evaluated to be 1.72, 1.76, and 1.70 eV for **P1**, **P2**, and **P3**, respectively, from the onsets of solid film absorption (Table 1).

The HOMO and LUMO energy levels of these three polymers were investigated by cyclic voltammetry (Figure S7, Supporting Information). The onset oxidation potential (E_{ox})/onset reduction potential (E_{red}) of **P1**, **P2**, and **P3** were 0.97/−1.24, 0.98/−1.29, and 0.95/−1.16 V vs Ag/Ag^+, respectively. From the values of E_{ox} and E_{red} of the polymers, the HOMO and the LUMO values as well as the electrochemical band gaps (E_g^{cv}) were calculated and also listed in Table 1 and Figure 2b. The HOMO energy levels of **P1**, **P2**, and **P3** are very close. It is well-known that inserting fluorine atoms can lower the HOMO level of polymer,[20] but introducing alkoxyl side groups can raise the HOMO level.[30,36] As a result, we inferred that these two kinds of influences could offset each other in polymer **P3**, and finally contributed a similar HOMO level in comparison with **P2** and **P3**. The LUMO energy levels of the polymers are all located within a suitable range (from −3.08 to −3.20 eV, Table1) and are significantly higher-lying than that of $PC_{71}BM$ (ca. −3.91 eV);[37,38] thus, efficient charge transfer (exciton dissociation) could be expected to occur in their corresponding devices. The electrochemical band gaps of the polymers are well matched with their optical band gaps within the experimental error.

Thermal Properties and X-ray Diffraction (XRD). The thermal properties of these polymers were studied by differential scanning colorimetry (DSC) and thermal gravimetric analysis (TGA) (Table 1 and Figure 3). **P3** showed a

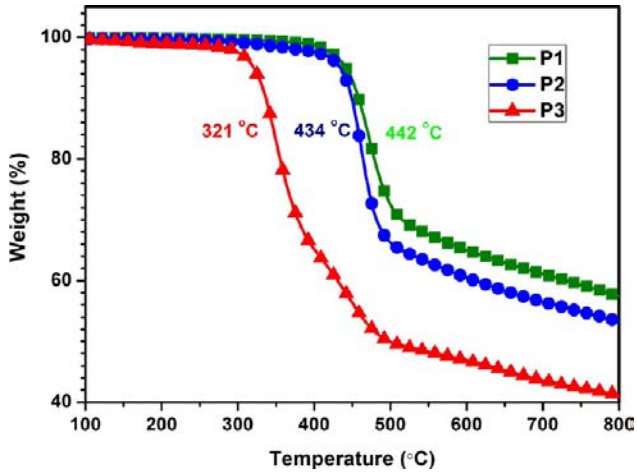

Figure 3. TGA curves of the polymers **P1**, **P2**, and **P3**.

glass transition at 138 °C, but both **P1** and **P2** did not show discernible glass transition. The thermal decomposition temperatures (5% weight loss) of **P1**, **P2**, and **P3** were 442, 434, and 321 °C, respectively, showing good thermal stability. It can be seen that the decomposition temperatures (T_d) at 5% weight loss of **P3** is lower than other polymers, because of the existence of the alkoxy group on BDT unit. Therefore, when the alkoxy groups were replaced by alkylthienyl groups, the stability of the polymers have been improved greatly.[30]

The powder X-ray diffraction spectra of polymers were carried out, and the curves are shown in Figure 4. The d_1-

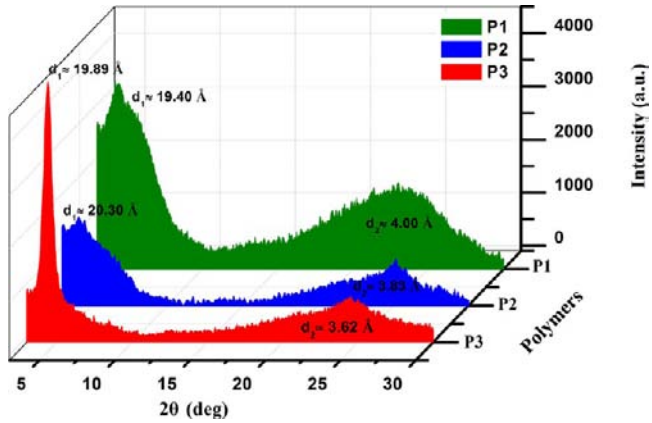

Figure 4. X-ray diffraction patterns of powdery polymers.

spacings corresponding to the in-plane spacing between polymer backbones are 19.40 Å for **P1**, 20.30 Å for **P2**, 19.89 Å for **P3**, and this kind of spacing is related to side chain length. The d_2-spacing (p-stacking distance) of 4.00 Å for **P1**, 3.83 Å for **P2**, and 3.62 Å for **P3** were also observed. Noticeably, as shown in Figure 4, the **P3** showed superior crystallization capability compared with **P1** and **P2**.

dx.doi.org/10.1021/ja409881g | J. Am. Chem. Soc. 2013, 135, 17060−17068

Hole Mobility. Hole mobilities of the polymers were measured by using the space-charge-limited current (SCLC) method in the direction perpendicular to the electrodes, and the linear fits for the plots of $\ln(I/V^2)$ versus $V^{1/2}$ based on the SCLC model are shown in Figure S8 (see Supporting Information).[39] The mobilities are estimated to be 4.9×10^{-3}, 6.3×10^{-3}, and 3.7×10^{-2} cm^2 V^{-1} s^{-1} for neat **P1**, **P2**, and **P3**, respectively. It is noteworthy that polymer containing oxygen atom unit showed higher hole mobility (3.7×10^{-2} cm^2 V^{-1} s^{-1}) than polymers with the thiophene unit (4.9×10^{-3} and 6.3×10^{-3} cm^2 V^{-1} s^{-1}). The inferior mobility value of **P1** may be attributed to the relative low solubility and poor film quality in comparison with **P2** and **P3**. The hole mobility in the polymer, however, could be influenced by morphology, field, recombination, or carrier density in photoactive layer under operating conditions. The mobility value of **P3** is comparable to or greater than those reported for typical high-PCE BHJ films,[7,40] in agreement with the high crystallization capability, ordered film microstructure, and close $\pi-\pi$ spacing. Such substantial mobility value of **P3** should partially account for high fill factor and short-circuit current density, although high hole mobility alone cannot guarantee high device performance.[41,42]

To gain insight into the differences in the performance of polymer:$PC_{71}BM$ BHJ devices with various blend ratios, the charge transport properties in blend films were also carried out in hole-only devices. The charge mobility can then be calculated to be 1.5×10^{-3} and 2.8×10^{-3} cm^2 V^{-1} s^{-1} for **P1**:$PC_{71}BM$ and **P2**:$PC_{71}BM$ (weight ratio of donor versus acceptor is 1:1.5), respectively. The charge carrier mobility data in these blend systems show the same trend but are lower than those in neat polymer cases, which may be came from the larger disorder in BHJ films. However, there is no significant hole mobility changes for polymer **P3** on blending with $PC_{71}BM$. The mobility values are 5.4×10^{-2}, 6.7×10^{-2}, and 4.0×10^{-2} cm^2 V^{-1} s^{-1} for the blends with 1:1, 1:1.5, and 1:2 weight ratios of **P3**:$PC_{71}BM$, respectively, indicating minimal disruption of polymer film microstructures after $PC_{71}BM$ blending. Among these mobility values of **P3**:$PC_{71}BM$ blends, the value for 1:1.5 donor/acceptor ratio are moderately higher than those in 1:1 and 1:2 donor/acceptor ratios, probably reflecting the suboptimal morphologies in the latter.

BHJ Solar Cell Performance and Morphology Characterization. Polymer solar cells were fabricated by employing **P1** or **P2** as a donor material and $PC_{71}BM$ as an acceptor material. The device architecture is ITO/PEDOT:PSS/Polymer:$PC_{71}BM$/Ca/Al and the device active area is 0.10 cm^2. In our experiments, more than 400 devices have been fabricated in total, and size dependence of PCE versus active area has not been found. Note that no processing additives were used at the time of spin coating and no postdeposition treatments such as thermal spin coating or annealing and solvent vapor treatment were employed, except special clarification for comparative experiments. The optimized device performance for **P1** and **P2** are shown in Figure 5, and the corresponding data are summarized in Table 2.

Device was fabricated from a blend of **P1** with $PC_{71}BM$ at 1:1.5 weight ratio harvested a V_{oc} of 0.68 V, a J_{sc} of 11.87 mA/cm^2, a modest FF of 55.2%, and correspondingly a PCE of 4.46%. Device made from **P2** with $PC_{71}BM$ at 1:1.5 weight ratio demonstrated a better result with a V_{oc} of 0.76 V, a J_{sc} of 13.17 mA/cm^2, and an improved FF of 61.9%. The PCE thus reached 6.20%. To our surprise, the device from **P2** showed

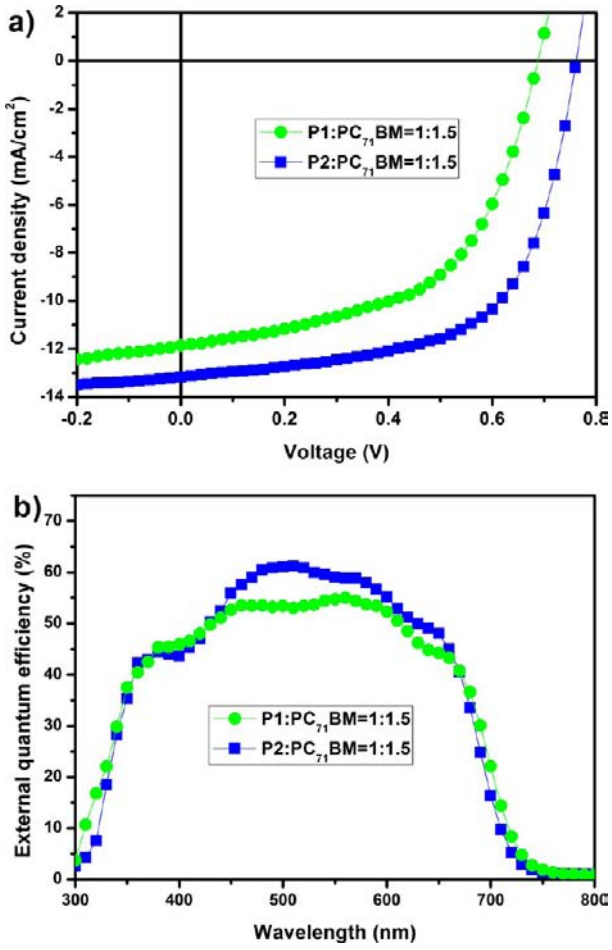

Figure 5. (a) Characteristic current density (J)−voltage (V) curves for the BHJ solar cells derived from **P1** (circle) and **P2** (square) under an illumination of AM 1.5G, 100 mW/cm^2. (b) The corresponding IPCE curves for (a).

Table 2. Characteristic Properties of BHJ Solar Cells Based on 1:1.5 Weight Ratio of Polymer and $PC_{71}BM$ for P1, P2 and P3, Respectively

polymer	thickness (nm)	V_{oc} (V)	J_{sc} (mA/cm^2)	FF (%)	PCE (%)[a]
P1	107	0.68	11.87	55.2	4.46[4.35]
P2	115	0.76	13.17	61.9	6.20[6.03]
P3	108	0.78	15.38	69.2	8.30[8.13]

[a]The values in square bracket stand for the average values of PCEs.

higher V_{oc} than the case from **P1**, although there is almost no difference in their HOMO energy levels. The possible explanation for this phenomenon should be linked to surface energy of polymer. It was well proved that the introduction of fluorine into the conjugated backbone would decrease the surface energy of fluorinated polymer.[24,43,44] Furthermore, the low solubility and poor film quality of **P1** should also contribute unfavorable factors for the low V_{oc}.[16,28] For J_{sc} and FF, the device from **P2** showed enhanced J_{sc} and FF, probably because of the combination of optimized morphology (vide infra) and preferable hole mobility of the blend. It is interesting to note that the PCE of 6.20% for a single junction device was achieved without using additives during the processing, which is a very unique property of **P2**. Figure 5b shows incident photon to current efficiency (IPCE) curves of BHJ devices based on **P1**

dx.doi.org/10.1021/ja409881g | J. Am. Chem. Soc. 2013, 135, 17060−17068

and **P2**, which are used to verify the measured J_{sc} values. A high photo-to-current response was obtained in the range from 300 to 700 nm for the **P2**-based device, thus suggesting a highly efficient photoconversion process.[45] This high IPCE response for the **P2** device, together with a high fill factor of 61.9%, possibly suggests balanced charge transport and improved active-layer morphology for the **P2** device. On the contrary, the IPCE of the **P1**-based device is low. Note that the theoretical J_{sc} values of **P1** and **P2** based devices obtained by integrating the product of the IPCE data in Figure 5b and the AM 1.5G solar spectrum are 11.63 and 12.96 mA/cm^2, respectively, which are in good agreement with the values (within 3% error) obtained from the $J-V$ characteristics (Figure 5 and Table 2).

The surface morphological structure of **P1**/$PC_{71}BM$ and **P2**/$PC_{71}BM$ blend films using tapping mode AFM are shown in Figure 6. The obtained root-mean-square roughness (RMS)

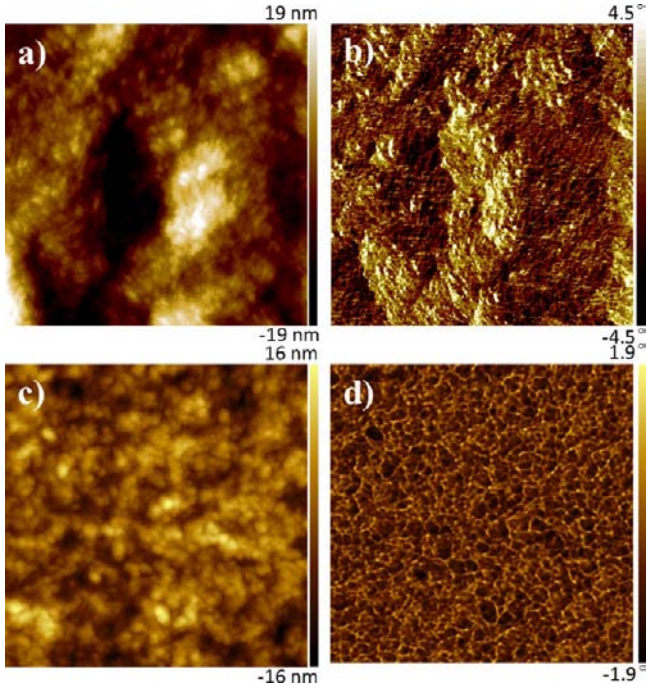

Figure 6. AFM topography (a, c) and phase images (b, d) of **P1**:$PC_{71}BM$ (upper) and **P2**:$PC_{71}BM$ (below) blend films, respectively. The scan size of the images is 5 μm × 5 μm.

values are 1.5 and 0.9 nm for the blend films from **P1** and **P2**, respectively, showing a decline trend. The phase image of the film from **P1** with $PC_{71}BM$ shows obscure domains without clear phase segregation; this may explain the modest FF of 55.2%. However, the blend film of **P2** and $PC_{71}BM$ has a more clear structure that exhibits an obviously continuous interpenetrating network. The structure is desired for better charge transport, and thus agrees with the enhanced FF of 61.9%.

In order to obtain optimized device performance, different weight ratios (1:1, 1:1.5, 1:2) of **P3**:$PC_{71}BM$ were used. The corresponding J_{sc}, V_{oc}, FF, and PCEs values derived from the $J-V$ curves and all of the relevant parameters are summarized in Table 3. As shown in Figure 7 and Table 3, the **P3**:$PC_{71}BM$ ratios, the effects of the additive, and photoactive layer thickness were carefully optimized. Overall, the best device performance was obtained in a 1:1.5 **P3**:$PC_{71}BM$ weight ratio spin-cast from *o*-dichlorobenzene with J_{sc} = 15.38 mA/cm^2, FF = 69.2%, V_{oc} = 0.78 V, and leading to a quite high PCE of

Table 3. Photovoltaic Characteristics of P3 in BHJ Solar Cells with Different Ratio of $PC_{71}BM$

P3:$PC_{71}BM$	thickness [nm]	V_{oc} [V]	J_{sc} [mA/cm^2]	FF [%]	PCE [%]
1:1	117	0.78	13.14	62.9	6.45[6.32][c]
1:1.5	108	0.78	15.38	69.2	8.30[8.13]
1:1.5	206	0.78	14.28	65.3	7.27[7.11]
1:1.5	330	0.78	13.75	61.2	6.56[6.35]
1:1.5[a]	126	0.76	12.74	55.6	5.38[5.24]
1:1.5[b]	97	0.78	14.26	67.8	7.54[7.27]
1:2	135	0.78	13.78	59.8	6.42[6.29]

[a]3% (v/v) 1,8-diiodooctane (DIO) as a processing additive. [b]$PC_{61}BM$ as an acceptor. [c]The values in square brackets indicate the average values of PCEs.

8.30%. The superior performance is associated with the high hole mobility and better nanoscale morphology of the interpenetrating network, allowing efficient exciton dissociation and enhancing charge carrier transportation. To the best of our knowledge, this high efficiency is the highest value reported from traditional single-junction BHJ PSCs without any post-treatment processes. In addition to the distinction in blend ratios, however, all devices based on **P3** exhibited high performance with PCEs > 6.10% under AM 1.5G illumination, within a thickness range of active layer from 100 to 330 nm, which facilitates the preparation of high-performance solar cells. With a weight ratio of 1:1 **P3**:$PC_{71}BM$, the device achieved a high PCE of 6.46% with J_{sc} = 13.14 mA/cm^2, FF = 63%, and V_{oc} = 0.78 V. Moreover, the device based on a weight ratio of 1:2 **P3**:$PC_{71}BM$ attained a moderate dropped performance with PCE of 6.43%, and corresponding parameters of J_{sc} = 13.78 mA/cm^2, FF = 59.83%, and V_{oc} = 0.78 V. Empirically, appropriate processing additive is an effective approach to further improve device performance. 1,8-diiodooctane (DIO) was selected as the additive benefiting from its high boiling point and ability to solvate the fullerenes. Unfortunately, the device of 1:1.5 **P3**:$PC_{71}BM$ with 3% (v/v) DIO additive could not accomplish an impressive PCE but performed comprehensive decline in operating parameters. It was found that the addition of DIO to the photoactive layer tended to reduce the V_{oc} of the devices to some extent. This phenomenon can be attributed to the lowering of charge-separated and charge-transfer-state energies upon additive addition.[46] The significant decrease in the J_{sc} and FF, when DIO was used, could be explained by the change in morphology of the blend, as we can see from the AFM images (Figure 8). It can be distinctly observed that the blend containing DIO exhibits rather rough surface with a RMS value of 1.8 nm and fairly large domain size over 100 nm, which is unfavorable for effective charge separation and consequently limits device performance. Nevertheless, in the case of without DIO, relatively smooth blend film along with appropriate domain size (<20 nm) are realized with RMS value of 0.6 nm, indicating better nanoscale separation between the polymer and fullerene and more efficient percolation pathways that can facilitate charge transport to the respective electrodes and thereby lead to optimized performance. Taking into account the fact that the result was obtained from as-cast photoactive layer that lacks processing additive or post-treatment, we believe there is still more room for further optimizations to realize optimum morphology of the active layer by precise regulation.

dx.doi.org/10.1021/ja409881g | J. Am. Chem. Soc. 2013, 135, 17060−17068

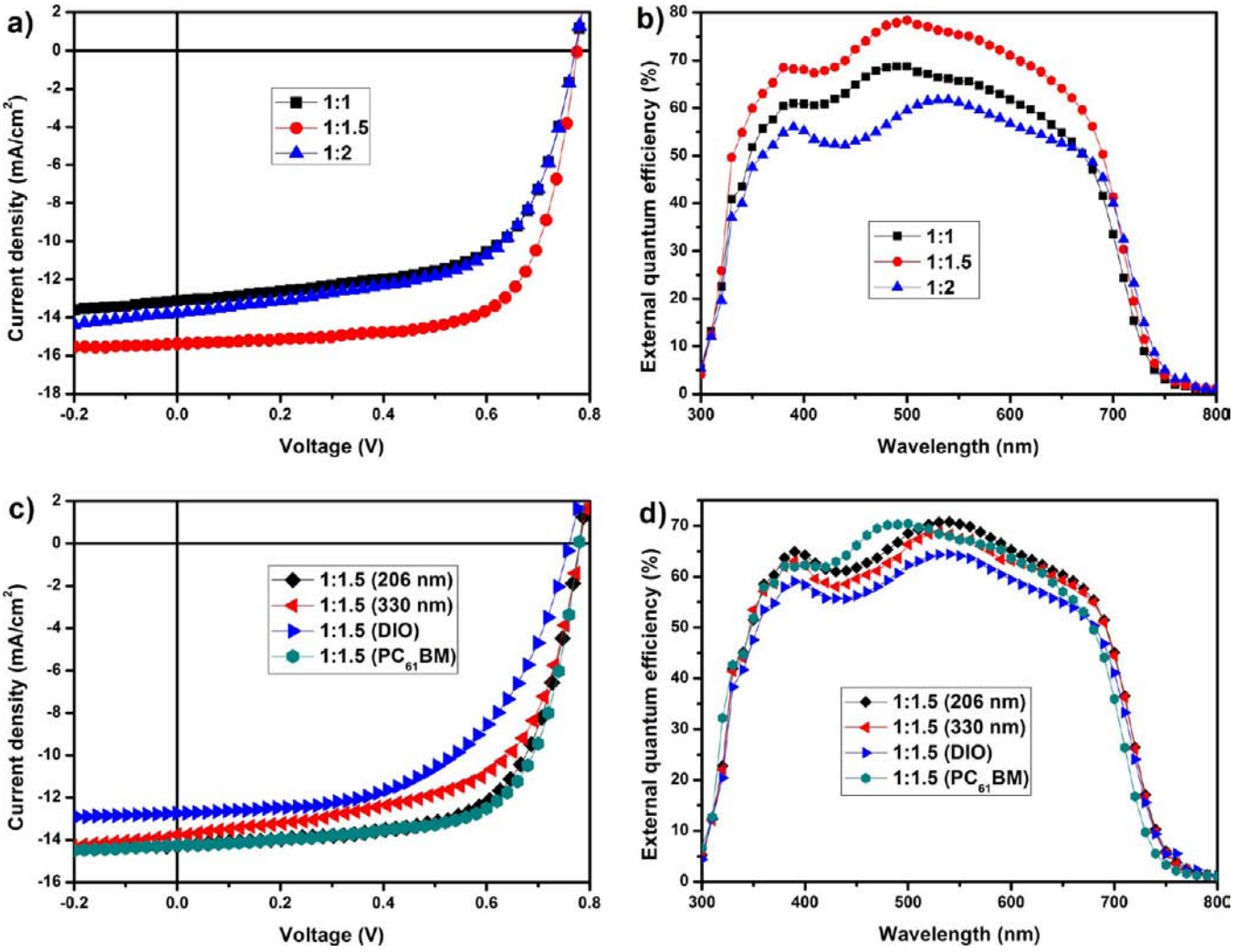

Figure 7. Current density (J)−voltage (V) curves of BHJ solar cells based on **P3** with various donor−acceptor ratios (a) and experiment conditions (c) under an illumination of AM 1.5G, 100 mW/cm^2; (b) and (d) are the corresponding external quantum efficiency spectra for (a) and (c), respectively.

Dramatically, the PCEs of the devices based on 1:1.5 weight ratio of **P3**:$PC_{71}BM$ still exhibited high values when thicker photoactive layers were employed (Figure 7c and Table 3). The J_{sc} and FF moderately decreased from 15.38 mA/cm^2 and 69.2% to 14.28 mA/cm^2 and 65.3%, respectively, as the active layer thickness doubled, with correspondingly a PCE of 7.27%. It should be noted that the FF value exceeded 60% even when the thickness of photoactive layer was more than 300 nm, which has been reported in only a few polymers.[18,26] As a result, the device with an active layer thickness of 330 nm accomplished a relatively high PCE of 6.56% (J_{sc} =13.75 mA/cm^2, FF = 61.2%, V_{oc} = 0.78 V). Our results should be significant for PSCs to meet commercial requirements in large-scale roll-to-roll processing. The insensitivity of PCE on photoactive layer thickness can facilitate manufacturing process by noncontact coating technologies, such as ultrasonic spray, slot die, and doctor blade. Similarly high photovoltaic performance was obtained when polymer **P3** was mixed with $PC_{61}BM$ instead of $PC_{71}BM$ (Figure 7c, Table 3), and the best cell demonstrated a PCE of 7.54%, with J_{sc} =14.26 mA/cm^2, FF = 67.8%, and V_{oc} = 0.78 V for a 97 nm thick active layer. Compared with the champion device, the drop in PCE primarily originates from weak light absorption in the visible region of $PC_{61}BM$. Figure 7b and 7d show the IPCE curves of devices based on various experiment conditions. It was identified that the J_{sc} measured from devices were in good agreement with integrated values (12.96, 15.26, and 13.44 mA/cm^2 for 1:1, 1:1.5 and 1:2 weight ratios of **P3**:$PC_{71}BM$, respectively; 13.71 and 13.57 mA/cm^2 for 206 and 330 nm thick blends of 1:1.5 **P3**:$PC_{71}BM$, respectively; 12.62 mA/cm^2 for 1:1.5 **P3**:$PC_{71}BM$ with DIO as an additive, and 14.13 mA/cm^2 for 1:1.5 **P3**:$PC_{61}BM$) of the IPCE data and the AM 1.5G solar spectrum (within 4% error).

3. CONCLUSION

In conclusion, the bulk branched alkoxy and alkylthienyl groups were introduced as substituents on BDT units to optimize the performance of conjugated polymers. As a result, a series of new conjugated polymers $PBDT_{TEH}$-$DT_{H}BTff$ (**P1**), $PBDT_{TEH}$-$DT_{EH}BTff$ (**P2**), $PBDT_{HDO}$-$DT_{H}BTff$ (**P3**) were developed. PCEs of 4.46, 6.20, and 8.30% were obtained for **P1**-, **P2**-, and **P3**-based PSCs within ∼100 nm thickness active layers under AM 1.5G illumination without any processing additives or post-treatments, respectively. Note that a record PCE of 8.3% was achieved in conventional single-junction BHJ polymer solar cell via a simple fabrication configuration without additional

dx.doi.org/10.1021/ja409881g | J. Am. Chem. Soc. 2013, 135, 17060−17068

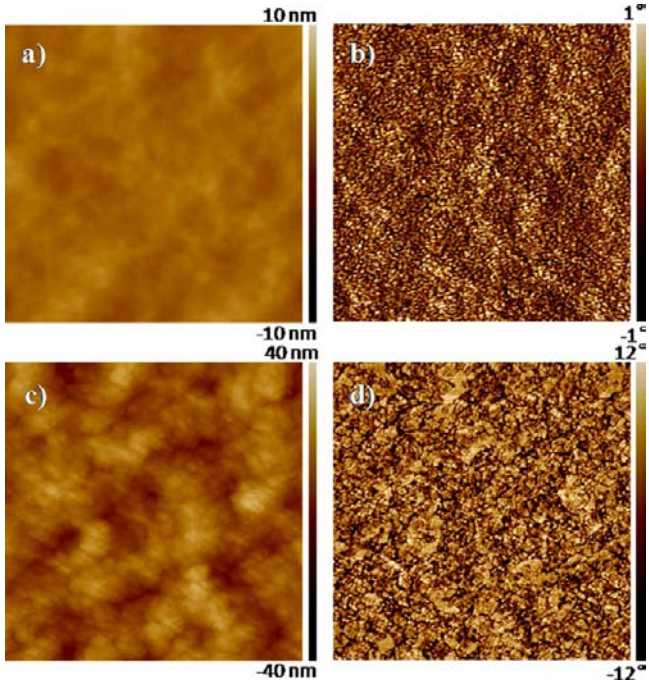

Figure 8. AFM topography and phase images (3 μm × 3 μm) of 1:1.5 **P3**:$PC_{71}BM$ blend films. Images on left side are the surface topography of the blend films without (a) and with (c) DIO as an additive; (b) and (d) are the corresponding phase images of (a) and (c).

modified layers, processing additives, or post-treatments. Within a wide thickness range (100−330 nm) of active layers, all devices based on **P3** showed relatively competitive PCE values (>6.4%) together with high fill factors (>61%). Furthermore, while the **P3** was mixed with $PC_{61}BM$ instead of $PC_{71}BM$, the device also exhibited a high PCE of 7.54%. These high efficiency behaviors and their low dependency to variations in thickness of active layers make polymer **P3** become a promising candidate in developing high-performance large-scale roll-to-roll industry printing applications of PSCs.

■ ASSOCIATED CONTENT

Supporting Information

Experimental details; synthesis of the monomers and polymers; cyclic voltammetry curves, hole mobility measurement; and AFM images. This material is available free of charge via the Internet at http://pubs.acs.org.

■ AUTHOR INFORMATION

Corresponding Author

chenzheng2013@jlu.edu.cn

Notes

The authors declare no competing financial interest.

■ ACKNOWLEDGMENTS

This work was financially supported by the National Natural Science Foundation of China (NSFC, Grant No. 21104077 and 51073066), Ph.D. Program Foundation of Ministry of Education of China (Grant No. 20120061110017), Jilin Provincial Education Department Foundation (Grant No. 2013-257), National High Technology Research and Development Program of China (863 Program, Grant No. 2012AA03A212), and the general research foundation of Jilin University (Grant No. 450060491410 and 450060491588).

■ REFERENCES

(1) Yu, G.; Gao, J.; Hummelen, J. C.; Wudl, F.; Heeger, A. J. *Science* **1995**, *270*, 1789.
(2) Dennler, G.; Scharber, M. C.; Brabec, C. J. *Adv. Mater.* **2009**, *21*, 1323.
(3) Li, G.; Zhu, R.; Yang, Y. *Nat. Photonics* **2012**, *6*, 153.
(4) Chen, H.-C.; Chen, Y.-H.; Liu, C.-C.; Chien, Y.-C.; Chou, S.-W.; Chou, P.-T. *Chem. Mater.* **2012**, *24*, 4766.
(5) Yang, T. B.; Wang, M.; Duan, C. H.; Hu, X. W.; Huang, L.; Peng, J. B.; Huang, F.; Gong, X. *Energy Environ. Sci.* **2012**, *5*, 8208.
(6) Small, C. E.; Chen, S.; Reynolds, J. R.; So, F.; Subbiah, J.; Amb, C. M.; Tsang, S.-W.; Lai, T.-H. *Nat. Photonics* **2012**, *6*, 115.
(7) He, Z.; Zhong, C.; Huang, X.; Wong, W. Y.; Wu, H.; Chen, L.; Su, S.; Cao, Y. *Adv. Mater.* **2011**, *23*, 4636.
(8) He, Z.; Zhong, C.; Su, S.; Xu, M.; Wu, H.; Cao, Y. *Nat. Photonics* **2012**, *6*, 591.
(9) Dou, L.; Chang, W. H.; Gao, J.; Chen, C. C.; You, J.; Yang, Y. *Adv. Mater.* **2013**, *25*, 825.
(10) Lu, L.; Luo, Z.; Xu, T.; Yu, L. *Nano Lett.* **2013**, *13*, 59.
(11) Dou, L.; Chen, C.-C.; Yoshimura, K.; Ohya, K.; Chang, W.-H.; Gao, J.; Liu, Y.; Richard, E.; Yang, Y. *Macromolecules* **2013**, *46*, 3384.
(12) Li, X.; Choy, W. C.; Huo, L.; Xie, F.; Sha, W. E.; Ding, B.; Guo, X.; Li, Y.; Hou, J.; You, J.; Yang, Y. *Adv. Mater.* **2012**, *24*, 3046.
(13) Cabanetos, C.; El Labban, A.; Bartelt, J. A.; Douglas, J. D.; Mateker, W. R.; Frechet, J. M.; McGehee, M. D.; Beaujuge, P. M. *J. Am. Chem. Soc.* **2013**, *135*, 4656.
(14) You, J.; Dou, L.; Yoshimura, K.; Kato, T.; Ohya, K.; Moriarty, T.; Emery, K.; Chen, C. C.; Gao, J.; Li, G.; Yang, Y. *Nat. Commun.* **2013**, *4*, 1446.
(15) Søndergaard, R.; Hösel, M.; Angmo, D.; Larsen-Olsen, T. T.; Krebs, F. C. *Mater. Today* **2012**, *15*, 36.
(16) Zhou, H.; Yang, L.; You, W. *Macromolecules* **2012**, *45*, 607.
(17) Blom, P. W. M.; Mihailetchi, V. D.; Koster, L. J. A.; Markov, D. E. *Adv. Mater.* **2007**, *19*, 1551.
(18) Li, W.; Hendriks, K. H.; Roelofs, W. S.; Kim, Y.; Wienk, M. M.; Janssen, R. A. *Adv. Mater.* **2013**, *25*, 3182.
(19) You, J.; Dou, L.; Yoshimura, K.; Kato, T.; Ohya, K.; Moriarty, T.; Emery, K.; Chen, C. C.; Gao, J.; Li, G.; Yang, Y. *Nat. Commun.* **2013**, *4*, 1446.
(20) Stuart, A. C.; Tumbleston, J. R.; Zhou, H.; Li, W.; Liu, S.; Ade, H.; You, W. *J. Am. Chem. Soc.* **2013**, *135*, 1806.
(21) Zhang, Y.; Zou, J.; Cheuh, C.-C.; Yip, H.-L.; Jen, A. K. Y. *Macromolecules* **2012**, *45*, 5427.
(22) Min, J.; Zhang, Z.-G.; Zhang, S.; Li, Y. *Chem. Mater.* **2012**, *24*, 3247.
(23) Albrecht, S.; Janietz, S.; Schindler, W.; Frisch, J.; Kurpiers, J.; Kniepert, J.; Inal, S.; Pingel, P.; Fostiropoulos, K.; Koch, N.; Neher, D. *J. Am. Chem. Soc.* **2012**, *134*, 14932.
(24) Zhou, H.; Yang, L.; Stuart, A. C.; Price, S. C.; Liu, S.; You, W. *Angew. Chem., Int. Ed.* **2011**, *50*, 2995.
(25) Zhang, Y.; Chien, S. C.; Chen, K. S.; Yip, H. L.; Sun, Y.; Davies, J. A.; Chen, F. C.; Jen, A. K. *Chem. Commun.* **2011**, *47*, 11026.
(26) Price, S. C.; Stuart, A. C.; Yang, L.; Zhou, H.; You, W. *J. Am. Chem. Soc.* **2011**, *133*, 4625.
(27) Peng, Q.; Liu, X.; Su, D.; Fu, G.; Xu, J.; Dai, L. *Adv. Mater.* **2011**, *23*, 4554.
(28) Li, Z.; Lu, J.; Tse, S.-C.; Zhou, J.; Du, X.; Tao, Y.; Ding, J. *J. Mater. Chem.* **2011**, *21*, 3226.
(29) Yang, L.; Zhou, H.; You, W. *J. Phys. Chem. C* **2010**, *114*, 16793.
(30) Huo, L.; Zhang, S.; Guo, X.; Xu, F.; Li, Y.; Hou, J. *Angew. Chem., Int. Ed.* **2011**, *50*, 9697.
(31) Sista, P.; Biewer, M. C.; Stefan, M. C. *Macromol. Rapid Commun.* **2012**, *33*, 9.
(32) Li, Y. *Acc. Chem. Res.* **2012**, *45*, 723.
(33) Zhou, E. J.; Cong, J. Z.; Hashimoto, K.; Tajima, K. *Macromolecules* **2013**, *46*, 763.
(34) Blouin, N.; Michaud, A.; Leclerc, M. *Adv. Mater.* **2007**, *19*, 2295.

(35) Blouin, N.; Michaud, A.; Gendron, D.; Wakim, S.; Blair, E.; Neagu-Plesu, R.; Belletete, M.; Durocher, G.; Tao, Y.; Leclerc, M. *J. Am. Chem. Soc.* **2008**, *130*, 732.
(36) Huo, L.; Hou, J. *Polym. Chem.* **2011**, *2*, 2453.
(37) He, Y.; Li, Y. *Phys. Chem. Chem. Phys.* **2011**, *13*, 1970.
(38) Huang, Y.; Guo, X.; Liu, F.; Huo, L.; Chen, Y.; Russell, T. P.; Han, C. C.; Li, Y.; Hou, J. *Adv. Mater.* **2012**, *24*, 3383.
(39) Murgatroyd, P. N. *J. Phys. D: Appl. Phys.* **1970**, *3*, 151.
(40) Guo, X.; Zhou, N.; Lou, S. J.; Hennek, J. W.; Ponce Ortiz, R.; Butler, M. R.; Boudreault, P. L.; Strzalka, J.; Morin, P. O.; Leclerc, M.; Lopez Navarrete, J. T.; Ratner, M. A.; Chen, L. X.; Chang, R. P.; Facchetti, A.; Marks, T. J. *J. Am. Chem. Soc.* **2012**, *134*, 18427.
(41) Qu, B.; Tian, D.; Cong, Z.; Wang, W.; An, Z.; Gao, C.; Gao, Z.; Yang, H.; Zhang, L.; Xiao, L.; Chen, Z.; Gong, Q. *J. Phys. Chem. C* **2013**, *117*, 3272.
(42) Parmer, J. E.; Mayer, A. C.; Hardin, B. E.; Scully, S. R.; McGehee, M. D.; Heeney, M.; McCulloch, I. *Appl. Phys. Lett.* **2008**, *92*, 113309.
(43) Kim, J. S.; Lee, Y.; Lee, J. H.; Park, J. H.; Kim, J. K.; Cho, K. *Adv. Mater.* **2010**, *22*, 1355.
(44) Brédas, J. L.; Heeger, A. J. *Chem. Phys. Lett.* **1994**, *217*, 507.
(45) Piliego, C.; Holcombe, T. W.; Douglas, J. D.; Woo, C. H.; Beaujuge, P. M.; Frechet, J. M. *J. Am. Chem. Soc.* **2010**, *132*, 7595.
(46) Nuzzo, D. D.; Aguirre, A.; Shahid, M.; Gevaerts, V. S.; Meskers, S. C.; Janssen, R. A. *Adv. Mater.* **2010**, *22*, 4321.